One-dimensional modeling of mechanical and friction losses distribution in a 4-stroke internal combustion engine

Bernardo Tormos
betormos@mot.upv.es

Jaime Martín
jaimardi@mot.upv.es

Diego Blanco-Cavero
dieblaca@mot.upv.es

Antonio J. Jiménez-Reyes[1]
anjire1@mot.upv.es

Instituto Universitario CMT-Motores Térmicos
Universitat Politècnica de València
Valencia, Spain 46022

ABSTRACT

Attending that road transport accounts between 15% - 18% of worldwide CO_2 emissions, the automotive sector has a deep commitment to mitigate global warming. Consequently, stricter regulations have been adopted by the European Union and worldwide to reduce that big impact. Approximately, 10% of the energy generated by fuel combustion in the engine is destined to the auxiliaries components activation and the movement of mechanical elements with relative motion between themselves. A reduction on that figure or alternatively a mechanical efficiency improvement can be directly translated on target alignment. The aim of this work is developing a model to predict the mechanical and friction losses and its distribution in a 4-stroke DI-Diesel engine and simulating different strategies which increment the engine efficiency. A 1D dimensional model has been developed and fitted in GT-Suite based on experimental results of a 1.6L Diesel engine. Additionally, a description of the tribological performance has been realized in different parts of the engine where friction is present. Finally, the engine friction maps have been broken down in

[1] Corresponding author

order to quantify the friction losses produced in the piston-ring assembly, crankshaft bearings and valvetrain.

1. INTRODUCTION

Internal combustion engines need to comply with stringent emission levels defined by governments and international organizations since road transport account for 15% to 18% of worldwide CO_2 emissions. The new European legislation imposes a reduction of the CO_2 (95 g/km until 2020 in fleet average [1]). A manner of reducing the emission of greenhouses gases is the reduction of the engine fuel consumption, a direct way to achieve this goal is to reduce the friction losses produced in the engine and consequently improving mechanical efficiency. Its contributions to the engine global energy balance is about 6% of the total energy introduced in the engine. Different ways have been taken in order to reduce the friction losses in engines such as: low viscosity oil usage [2], different surface texture [3] and coating and short engine oil warm-up period [4].

Modeling the mechanical losses that occurs in the engine is a useful task as first step to reduce the friction losses since it helps (i) to quantify the friction and (ii) to know the different contribution of each rubbing pair in ICE. In [5], Taylor proposed a 1D model to predict the friction losses in engines. This work uses the Mobility Approach to calculate the friction losses produced in the journal bearing, the authors estimate the load in engine bearings by means of Dubois and Ocvirk [6] short bearing approximation which provides a good approximation to the full solution and Reynolds equation to predict the friction losses in the piston-assembly. Taraza [7] proposed a model based in the Stricbeck diagram. More focused works are found in [8–12], in which the authors

proposed a model for piston ring assembly which includes different effect such as: bore distortion, cavitation and surface texture.

In journal bearings different authors propose the Reynolds equation and solving the energy equation [13], [14]. In these works, the mobility approach is considered to obtain the friction losses in journal bearings estimating the load in the engine bearing.

Valvetrain friction gains importance at low engine speed [15]. In order to reduce the friction losses, different strategies have been followed such as surface texture in cam-tappet configuration or cam-roller configuration, both alternatives have shown significative friction reduction [16]. Several authors predict the friction contact force in cam-roller camshaft by means of Hertz contact model. Currently, different models are proposed to calculate the minimum oil film thickness present between cam lobe and follower considering linear contact [17–19].

The 1D model presented in this work has been fitted for a DI-Diesel engine. Nevertheless, it is possible to apply the same methodology to know the mechanical losses of any ICE. To set up the model apart of some engine geometric data it is only necessary to carry out standard experimental tests in order to obtain some variables of the engine required by the model, such as: in-cylinder pressure, oil , piston, rings, cylinder working temperatures...

Thus, the work presented shows a complete model that predicts mechanical losses and their distribution in an ICE. In addition, it allows to know in detail the phenomena of friction in the piston-ring assembly, bearings and valvetrain. The model is a useful tool to asses different strategies to increase the efficiency of the internal combustion engine and thus, to reduce the emissions of CO_2 emitted to the ambient.

Also, different combustion engines can be introduced in the model developed. This tool facilitates the study of mechanical friction losses and its improvement in any internal combustion engine, both 2-stroke and 4-stroke

2. THEORETICAL AND EXPERIMENTAL TOOLS

2.1. GT-Suite

In order to calculate the friction losses in DI-Diesel engine GT-Suite software has been used. GT-Suite is a well-known software to simulate different engine performance. Different authors use GT-Suite to predict mechanical losses and tribology performance in ICE rubbing pairs [20], [21].

2.2. Experimental setup

In order to obtain the experimental FMEP in a DI-Diesel engine, whose main characteristics are in Tab. 1, the net IMEP method has been used in an instrumented test cell. The net IMEP is computed from the net indicated work integrated along the complete thermodynamic cycle. FMEP thus represents the friction losses due to rubbing between mechanical parts and accessories and does not include pumping work. The in-cylinder pressure has been measured with 4 AVL GH13P piezo- electric transducers installed at the glow plug hole of each cylinder. The signal acquired by the piezo-electric transducers was conditioned by means of a Kistler 5011B amplifier. This acquisition system was calibrated according to [22].

Mean temperatures of the intake and exhaust gases, coolant and lubricant were measured with a K-type thermocouple. The injected fuel was measured with an AVL 733S fuel meter, the air flow was measured with a DN80 sensiflow, the blow-by leakage, necessary to calculate the force produced in the rings was measured with an AVL blow-by-meter.

The acquisition and control of the low frequency signals was performed with STARS. The instantaneous in-cylinder pressure signals were acquired by means of a Yokogawa DL708E Oscillographic recorder with 16 A/D converter module.

Finally, in order to acquire the parameters registered by the engine control unit (ECU), the ETAS INCA software was used.

3. MODEL DESCRIPTION

3.1. Engine Oil Properties

Table 2 shows the main lubricant properties of the oil used in the engine.

To simulate the dynamic viscosity at different temperatures, the Vogel equation has been considered.

$$\mu = \kappa \exp\left(\frac{\theta_1}{\theta_2 + T}\right) \tag{1}$$

Where κ, θ_1 and θ_2 are constant for the lubricant used. Moreover, in order to calculate the lubricant density GT-Suite uses next expression [23]:

$$\rho(P,T) = a_0 + \frac{[P + a_1 T + a_2]^{(a_3+1)}}{(a_3+1)} + P[a_4 T^{a_5} + a_6] + a_7\sqrt{T} \tag{2}$$

Where T is the oil temperature in Kelvin, P is the oil pressure in bar and a_i are fitting constants of the oil. The kinematic viscosity is calculated as the ratio between the dynamic viscosity and density of the lubricant.

Both in piston-ring and journal bearing, iso-viscous lubricant behavior is considered due to relative low pressures in that part is assumed according to [24]. However, in camshaft model, the lubricant acts in a piezo-viscous manner, and it is explained in section 3.5

3.2. Piston-ring pack assembly model

Due to the importance of the friction in the global fuel consumption of the engine a model which quantify the power losses in the piston ring has been implemented. The friction caused by piston-ring assembly in an ICE is estimated between 50-75% [25] of the total friction losses produced. To achieve this goal a ring radial force balance and a force toroidal moment balance in the piston-ring pack is realized. In Fig. 1 a graphic representation of the forces balance is represented. According to [26] the equations which governs the process are:

$$M\frac{d^2r}{dt^2} = F_p + F_t - F_{oil} - F_{asp} \tag{3}$$

$$I_{ring}\frac{d^2\theta}{dt^2} = F_g(R_g - R_r) + F_p(R_g - R_r) + F_{cf}(R_c - R_r) + M_{cn} - K_t\theta - C_t\frac{d\theta}{dt} \tag{4}$$

Where F_p is the pressure force of the blow-by gas produced behind and the upper and bottom land of the ring; F_t is the force generated as consequence of the ring tension and the radius change due to the thermal expansion suffered by the ring; F_g is the reaction force caused by the contact between the ring and the cylinder groove; R_g is the radial distance between the piston center and ring groove; R_c is the cylinder radius; Rr is the ring radius ;M_{cn} is the friction force moment in the cylinder; K_t and C_t are the elastic and damping internal coefficient of the ring respectively.

In pistons-rings assemblies the mixed and hydrodynamic lubrication regimes are observed [27], [28] thus the friction force is calculated as:

$$F_{frc} = F_{f,hyd} + C_f F_{f,asp} \tag{5}$$

Being,

$$F_{f,hyd} = \int_{z_1}^{z_2} \left[\frac{\mu U}{h} - \frac{1}{2} h \frac{dP_{hyd}}{dz} \right] dz \quad (6)$$

And

$$F_{f,asp} = \int_{z_1}^{z_2} P_{asp} dz \quad (7)$$

C_f is the dry friction coefficient, attending that the materials considered are steel and cast-iron a value of 0.215 is selected. As much contact pressure as hydrodynamic pressure is integrated along the shape of the ring (z) therefore the ring profile must be known. Fig. 2 represents the different ring profiles used in the engine under study where the measures are given in millimeters.

To calculate the pressure produced by oil film in the ring face, the Average Reynolds equation with Patir and Cheng factors is used [29], [30].

$$\frac{\partial}{\partial x}\left(\Phi_p h_t^3 \frac{\partial P}{\partial x} \right) = 6U\mu \left(\frac{\partial h_t}{\partial x} + \sigma \frac{\partial \Phi_s}{\partial x} \right) + 12\mu \frac{\partial h_t}{\partial t} \quad (8)$$

Where h_t is the average local film thickness calculated from the instantaneous local film thickness and the composite roughness of the surfaces [23], U is the piston velocity during the cycle, μ is the dynamic viscosity of the oil which depends on the oil temperature. The oil temperature is considered as an average value of temperature between cylinder and ring, calculated according to [31] [32]. Using the experimental cylinder measured temperature, the proposed model can infer different temperatures on the piston-ring assembly. In Fig. 3, the cylinder wall temperature calculated at different engine speed and full load condition in function of its axial position can be observed, moreover the rings temperatures are shown at fixed engine speed changing the load.

The Patir and Cheng factors are included in the Reynolds equation to determine the effects of surface roughness in terms of pressure and shear flow factors. The surface characteristic γ is defined as the ratio of x (asperity width) and y (asperity height) correlation lengths. In this work isotropic roughness structure is considered (γ = 1).

The mixed lubrication regime in the piston-ring pack is given when $1 \leq h/\sigma < 3$ [33]. It occurs near the TDC in the combustion part of the cycle. To calculate the contact pressure in the piston-ring, the Greenwood-Tripp Model [34] is used. In the Greenwood-Tripp model spherical shape of the asperity is assumed with constant radius β. Moreover, the peaks are uniformly distributed with density η of peaks per area unit. Considering the assumptions proposed by G-T, the pressure contact is calculated as:

$$P_{asp} = \frac{16\sqrt{2}}{15}\pi(\sigma\beta_0\eta)^2 E\sqrt{\frac{\sigma}{\beta_0}}f_{\frac{5}{2}}\left(\frac{h}{\sigma}\right) \tag{9}$$

And

$$f_{\frac{5}{2}} = \frac{1}{\sqrt{2\pi}}\int_x^{\infty}(s-x)^{5/2}e^{\left(\frac{-s^2}{2}\right)}ds \tag{10}$$

Where h is the local film thickness between both surfaces. σ is the composite roughness height deviation $\sigma = \sqrt{\sigma_1 + \sigma_2}$; $\eta = \frac{\eta_1+\eta_2}{2}$; $\beta_0 = \left(\frac{1}{\beta_1}+\frac{1}{\beta_2}\right)^{-1}$ and E is the elasticity modulus combined with the Poisson ratio of the material ν such as $\frac{1}{E} = \left(\frac{1-\upsilon^2}{E_1}+\frac{1-\upsilon^2}{E_2}\right)$. It is assumed that the height of the asperities is fitted by Gaussian distribution. In this work the values adopted are shown in Tab. 3 according to [35].

Finally, partially-flooded condition in the piston-cylinder assembly is applied. This assumption is cause of considering that the oil supply available to lubricate next ring is a combination of the oil film left on the liner by the preceding ring and any

possible amount of accumulated oil at a specified crank angle [36] [37]. The immediate consequence is an increase of the contact pressure. However, the fully-flooded condition is managed by oil control ring during the downstroke because the oil deposited in the liner takes all over thickness available in the assembly. Figure 4 shows, the oil film thickness available for each ring qualitatively in the downstroke. The dashed line represents the oil film available in case of considering fully-flooded condition.

3.3. Piston skirt model

To simulate friction losses in skirt-cylinder assembly a similar procedure as described above is used. The solution used is quite approximate with no thermoelastic deformation of the skirt, the contact as explained in [38] is thermo- eslatohydrodinamic and a 2D Reynolds solution with deformed profile would be necessary in order to obtain a detailed solution. However, the solution adopted is a good approximation to the tribological phenomena which occurs in the engine skirt according to [39]. Average Reynolds equation with cylindrical coordinates and Greenwood-Tripp model to calculate hydrodynamic pressure and contact pressure is used.

Moreover, the piston secondary motion is calculated both major plane of the piston skirt and minor plane of the piston skirt as explained in [40]. Also, in this work no axial deformation of the skirt is considered, thus, the skirt is adopted as a solid body. A proper dynamic analysis can be found in [41].

3.4. Journal Bearings model

In order to estimate the friction power losses in engine journal bearings the Mobility method is adopted [42]. Rigid bearing model with parallel axis (no tilt) is used here. This model considers that three are the factors which contribute to total torque

and friction power loss in the bearing including shear, squeeze and contact whose expression is:

$$N_{total} = N_{shear} + N_{squeeze} + N_{contact} \quad (11)$$

The shear term is the power required to shear the fluid due to relative rotation between the journal and shell and is calculated with next relation.

$$N_{shear} = \frac{2\pi R^3 L\mu\left|\omega_j - \omega_b\right|^2}{\sqrt{c^2 - \varepsilon^3}} + \left(\varepsilon_x F_y - \varepsilon_y F_x\right)\left(\frac{\omega_j + \omega_b}{2}\right) \quad (12)$$

First term of the equation represent the effect described above, where R represent the bearing radius ; L represents the bearing width; μ is the lubricant viscosity at work temperature; ω_j and ω_b are the angular velocity of the journal and bearing respectively; c is the radial clearance between the journal and bearing and ε is the eccentricity calculated according to [42]. Second term of the Eq. 12 is generated due to the journal and bearing center misalignment. Since the reaction forces are equal and opposite but applied at different locations, they generate a moment couple located at the midpoint of the journal center and bearing center [43].

The squeeze term in Eq. 11 is due to the force of the journal moving with a certain linear velocity as well because of this phenomena no torque is generated [44].

$$N_{squeeze} = \frac{d\varepsilon_x}{dt} F_x + \frac{d\varepsilon_y}{dt} F_y \quad (13)$$

Finally, the contact force generated in the journal bearing is calculated with the Greenwood-Tripp model previously described. In Tab. 4 the parameters used to simulate friction force in journal-bearing are summarized.

3.5. Valvetrain model

The modeled valvetrain of the engine presented in this work is a direct acting cam and follower with finger-follower configuration. The main advantage of this

configuration is a reduction of the friction coefficient between the cam and the follower. The main part of the friction losses is due to the direct contact between the cam and follower which during most of the cycle is given under mixed and boundary lubrication regime. To simulate the pressure, contact the Hertzian model is used. The Hertzian model assumes two cylinders in contact with an uniform pressure distribution in the axial direction [45].

$$P_{Hertz} = 0.399 w^{0.5} E^{0.5} l^{-0.5} r^{-0.5} \sqrt{1 - \left(\frac{x}{1.598 w^{0.5} E^{-0.5} l^{-0.5} r^{0.5}}\right)^2} \quad (14)$$

Where P_{Hertz} is the pressure along width x; w is the total normal load applied; l is the axial length of the contact; r is the combined radius of both surfaces and E is the Young's modulus presented on Tab. 3

Also, a contact deformation model is used to predict the deformation between both surfaces:

$$\delta = 1.2599 w^{2/3} E^{-2/3} r^{-1/3} \quad (15)$$

The friction force carried by the camshaft can be expressed as:

$$F_{fr,v} = F_b + F_v \quad (16)$$

Where F_b, the boundary component can be written as:

$$F_b = \tau_0 A_a + m P_a \quad (17)$$

Being τ_0 the Eyring Shear Stress considered 2.5 MPa in this work. m represents the pressure coefficient of the boundary: 0.17 [46]; A_a and P_a is the area and pressure carried out by the asperities, modeled as explained in [46]

On the other hand, the viscous component of equation 16, F_v, is modeled according to [47]:

$$F_v = \tau(A - A_a) \tag{18}$$

where τ is de shear stress of lubricant. Depending on the oil film thickness, Newtonian or non-Newtonian behavior oil film will occur. The limit is the Eyring Shear. If the shear stress is lower than this value, can be evaluated as:

$$\tau = \frac{\mu_{Roeland} u_s}{h_0} \tag{19}$$

Where u_s is the sliding velocity, $\mu_{Roeland}$ is the Roeland equation effect of pressure on viscosity expressed as:

$$\mu_{Roeland} = \mu_{ambient} e^{\left[\left(1+\frac{p}{p_r}\right)^z - 1\right]\ln\left(\frac{\mu_{ambient}}{\mu_\infty}\right)} \tag{20}$$

Being

$$z = \frac{\alpha p_r}{\ln\left(\frac{\mu_{ambient}}{\mu_\infty}\right)} \tag{21}$$

Where α is the pressure-viscosity coefficient $15 \cdot 10^{-9}$ 1/Pa. p is the oil film pressure; p_r is a constant pressure $1.96 \cdot 10^8$ Pa; μ_∞ is the viscosity constant $6.315 \cdot 10^{-5}$ Pa·s as explained in [48].

In the case that τ would be higher than Eyring Shear, is modeled as:

$$\tau = \tau_0 + \kappa \frac{F_{N,valv} - P_a}{A - A_a} \tag{22}$$

Being κ the rate of change of shear stress with pressure, taking a value of 0.08 [47] and $F_{N,valv}$ the normal force acting in the contact.

Finally, the solution adopted to calculate the minimum oil film thickness is proposed by Moes [49].

$$h_{ctr} = \left[\left(H_{RI}^{2.333} + H_{EI}^{2.33}\right)^{0.429s} + \left(H_{RP}^{3.5} + H_{EP}^{3.5}\right)^{0.286s}\right]^{s^{-1}} \tag{23}$$

The Moes equation take into account the four limits present in the equation. Subscript RI is the rigid-viscous limit; Subscript RP is the rigid-piezoviscous limit;

Subscript EI is the elastic-isoviscous limit and the subscript EP is the elastic- piezoviscous limit of the oil.

3.6. Engine auxiliaries models

In this section the fuel, coolant and oil pumps consumption have been estimated. To calculate the drive power of each of them, the methodology proposed in [50] has been used.

In the case of oil pump losses, the expression which models the mechanical losses is:

$$N_{oil} = \frac{k_{1,oil} n \Delta P_{oil,max}}{\mu_{oil}} \tag{24}$$

if $\Delta P_{oil} = \Delta P_{oil,max}$

Furthermore, if the pressure provided by the pump if not the maximum pressure, the oil pump mechanical losses are modeled as:

$$N_{oil} = \frac{\left(k_{1,oil} n\right)^3}{\mu_{oil}} \left(\frac{k_{2,oil} \mu_{oil}}{k_{1,oil}}\right)^{k_{3,oil}} \tag{25}$$

The fuel pump power depends, basically, on the fuel mass flow rate through the pump and the pressure rise acquired. With this consideration, the expression which determines the fuel pump power is:

$$N_{fuel} = \frac{k_{1,f} P_{rail} m_f^{k_{2,f}}}{\mu_{fuel}} \tag{26}$$

To complete the auxiliary losses the coolant pump losses are modeled. Considering the pressure rises and the pump mass flow. Operating, the expression of the pump power can be modeled as:

$$N_{cool} = \frac{k_{1,cool}\left(k_{2,cool}n\right)^3}{\mu_{cool}} \quad (27)$$

The constants k_i have been fitted experimentally with available maps of the pumps and experimental data from the engine at different operating conditions. Thus, the coefficients shown in Tab. 5 were obtained.

4. RESULTS AND DISCUSSION

4.1. Model validation

The model results are presented in a wide range of load and engine speed, covering most of the engine map.

Figure 5 shows the correlation achieved for the engine, comparing experimental versus modeled results. It is interesting to highlight that the model results agree well with the experimental results, so, the results from simulation is highly representative of the mechanical losses given in the engine.

Moreover, a mechanical losses distribution has been represented in the engine. According to [25] the mechanical losses in the piston rings can reach until 75%, the friction in bearings until 20%, in valvetrain until 20% and auxiliaries until 25%. In the present work, the simulated distribution of the mechanical losses achieved in the 4-stroke engine is shown in Fig. 6.

It can be observed that the journal bearing and valvetrain friction percentage decrease with the engine load when keeping engine speed. The main reason is the effect of the in-cylinder pressure reached in the combustion chamber. The higher the load is, the higher the pressure behind the rings is, therefore the friction losses in the piston ring-assembly increases more than the friction losses both at the journal bearing and

valvetrain. Moreover, the auxiliary losses increase with the load as well. The main reason is the pressure in oil circuit and injector increase. Also, the auxiliary losses increase with the engine speed.

4.2. Piston-ring assembly

The friction force in the piston assembly depends directly on the normal load applied behind the ring. That load are the ring tension and the gas pressure on the ring, considering the pressure presents in the groove and upper and bottom lands. In Fig. 7 the pressure in the interface ring-cylinder for fired ring is shown. The upper and groove pressure is considered as the pressure above the ring and the land pressure is calculated as the blow-by model presented in [51].

The in-cylinder pressure increases with load. As consequence, it is observed that the MOFT in the fired ring-cylinder interface also diminishes with the load, as shown in Fig. 8. The effect of the engine speed in the MOFT is represented in Fig. 8 at same load. As it can be seen, the higher engine speed is, the higher MOFT is, principally due to achieving the same load, if the engine speed is lower, the in-cylinder pressure raises, hence, the ring load and the oil temperature rise. Because of this phenomena the viscosity of the oil decrease.

The effect of increasing load in the engine lead to oil film smaller as a cause of the increase of the pressure supported by the ring. Near combustion TDC, the piston-ring assembly achieve the boundary lubrication regime. Considering that the temperature of the oil is calculated as the average temperature between the ring and the cylinder wall, in that point of the cycle is maximum and the oil viscosity is minimum, so, the film thickness is minimum close to TDC. The coefficient of friction is represented in TDC environment in Fig. 9, where the smaller minimum oil film thickness is, the larger

friction coefficient becomes. After TDC the maximum load supported by rings is achieved, however the minimum oil film thickness is not reach at that point. Attending to the change of movement of the ring is considered instantaneous and equal to the change of the position of the piston the twist and consequently the instantaneous velocity of the ring will be higher than real behavior and it is not a realistic approximation to the real performance produced, as it is explained in [52]. Moreover, the available oil film thickness for fired ring just after TDC is represented in Fig. 10. As it has been explained, as a result of the higher twist, the major oil film thickness available at ring leading point is given at the full load operating point in the leading of the ring.

On the other hand, during most of the cycle, mixed lubrication is the predominant regime as Fig. 8 shows. In spite of maximum friction force is given at the end of the compression stroke, the maximum friction power loss is reached during the combustion stroke. that occurs because the piston speed in the angle where the friction force is maximum is higher in the combustion stroke than the compression stroke. The phenomena is shown in Fig. 11. Moreover, the more engine load at low speed, the more important effect of the piston-assembly in the engine friction losses because of friction losses in bearings and valvetrain depends, basically, on the engine speed.

4.3. Piston skirt

Piston skirt is considered working only in hydrodynamic lubrication regime, thus only 10% of the piston friction losses is due to the skirt because of the different load supported and lubrication regime in the rings and skirt. Figure 12 shows the friction power losses produced in the piston skirt at 1250 rpm.

Considering that the pressure in the piston skirt is the atmospheric pressure both major thrust and minor thrust due to the crankcase pressure is, approximately

atmospheric pressure, the normal force remains constant integrated along a cycle, thus the higher oil temperature is, the lower friction losses is due to a minor friction coefficient in the Stribeck curve.

4.4. Journal Bearings

In contrast to lubrication regime in piston assembly, journal bearings are designed to work in hydrodynamic regime in order to reduce potential wear [53]. Also, the crankshaft it is considered as a rigid body. The main bearing situated in the middle of the crankshaft support the major load of all main bearing due to its location. That bearing, receives directly the forces resulting from the cylinder 2 and 3 and 1 and 4 to a lesser extent. However, the main bearing situated in the end of the crankshaft only support the load coming from the cylinder close to it. These effects can be observed in the minimum oil film thickness at same load and engine speed shown in Fig. 13. Despite being the maximum load point, the main bearings stay in hydrodynamic regime during all the cycle.

Also, the minimum oil film thickness in cod-rod bearings is represented. The load supported by the cod-rod bearing is higher than main bearing due to the load is transmitted directly by the con-rod in the radial direction. However, in main bearing is not transmitted directly by the axial direction of the pressure. In spite of this effects, the minor oil film thickness is slightly higher than main bearing because of con-rod bearing is wider than main bearing and the load per length unit is minor. The orbit followed by bearing and journal and minimum oil film thickness in the rubbing pair is represented in Fig. 14.

4.5. Valvetrain

The cam-roller follower mechanism has a lower coefficient of friction (rolling) than the friction coefficient of the direct- acting (sliding) mechanism. But there are other components that compute total friction losses in the camshaft such as: bearings, valve stem... Although the rolling coefficient decreases friction, comparatively the contact between cam and follower (independently of which mechanism is considered) represents the major contribution to the total valve train system friction compared with other components such as camshaft bearings or valve stems. Moreover, in the moment of the contact boundary regime is achieved, taking more importance the superficial finishing in order to reduce the friction losses. The friction losses occurring during intake period are a little bit lower than during the exhaust stroke, because the in-cylinder pressure in the combustion chamber is higher in this part of the cycle.

Figure 15 shows the friction losses in cam-follower contact. As can be seen the engine load does not affects significantly the friction losses in the valvetrain. In the other hand, the EHD minimum oil film thickness is represented, when intake valve occurs the cam lobe acts on the roller, due to the necessary force to move the valve, the minimum oil film thickness is achieved. In this condition boundary regime is achieved.

4.6. Friction engine maps

The friction maps of each tribology pair are represented in Fig. 16.

In piston assembly maps the friction losses mainly depends on the engine load this effect has been justified because of the higher in-cylinder pressure. On the other hand, if the engine speed increases at the same load, the oil temperature increase and the oil viscosity decrease, increasing the friction coefficient more slowly accordingly to the Stribeck curve. Also, at same engine speed if the load rises the oil viscosity decreases,

the blow-by pressure, and, consequently the normal load in rings increase with speed and load, the effect is an increase directly of the friction coefficient.

Regarding the bearings, due to hydrodynamic regime, the engine speed is determinant in the friction losses, due to the gradient of the Stribeck curve in hydrodynamic regime and, consequently, the friction losses grows with the relative velocity.

Finally, in the camshaft map the contour can be justified due to the lubrication regime in the camshaft. At medium load and engine speed the mixed lubrication is achieved, and thus, the coefficient of friction is minimum leading to the relative lower friction in this part of the engine map. However, at high speed and high load the oil viscosity descends, and the camshaft enter to boundary lubrication, the same phenomena occurs at low regime speed and high load, growing the friction coefficient. At low regime speed and low load, the predominant lubrication regime is mixed, for this reason if the engine speed is increased at low load, the camshaft friction increases more gently than at high load.

5. CONCLUSIONS

Mechanical losses in a DI-Diesel engine have been modeled with a 1D friction model. The model correlated in this work permit predicting the oil performance under different engine operations. So, it can be known the mechanical losses produced in an ICE changing some inputs parameters such as geometry and the oil properties which helps to understand the friction phenomena.

In hydrodynamic regime the lower the oil film thickness is, the lower the friction produced is. As this type of regime takes place in bearings which are design to avoid abrasive wear, the direct way to improve the mechanical efficiency in journal bearing is

reducing the dynamic viscosity of the engine oil. In the other hand, the mixed regime achieved in piston- ring assembly lead to the necessity of finding a compromise considering the different conditions of the complete engine map. When the load increases, the boundary regime is achieved in the piston-ring assembly producing and increase of the friction losses and a higher wear in the piston rings; hence decreasing the dynamic viscosity of the engine oil is a counter-productive strategy, because the film thickness in that case is lower and the contact pressure increase. However, at low load, decreasing the oil viscosity can produce several consequences in bearings due to the film thickness decreases and the abrasive wear could occur, although at low load, decreasing the oil viscosity reduces the friction losses in piston-ring assembly where the most of the friction is produced in that rubbing pair.

In valvetrain the boundary regime is achieved when the contact exists. So, the main goal in order to reduce the friction losses is improving the surface texture in both cam and follower.

ACKNOWLEDGMENT

This research has been partially funded by the Spanish government under the grant agreement TRA2017-89894-R.

NOMENCLATURE

1D	One Dimensional
BDC	Bottom Dead Center
c	Radial clearance between journal and bearing (mm)
CoF	Coefficient of Friction
DI	Direct Injection
E	Young's modulus (Pa)
EHD	Elastohydrodynamic
F	Force (N)
f	Gaussian distribution
FMEP	Friction Mean Effective Pressure (bar)
G-T	Greenwood-Tripp
h	Instantaneous local film thickness (m)
h_t	Average local film thickness (m)
ICE	Internal Combustion Engines
IMEP	Indicated Mean Effective Pressure (bar)
k	Calibration constants
L	Bearing Width (m)
M	Mass of piston ring (kg)
MOFT	Minimum oil film thickness

n	Engine speed (1/s)
N	Power (W)
P	Pressure (Pa)
R	Bearing Radius (m)
t	Time (s)
T	Temperature (K)
TDC	Top Dead Center
U	Piston Velocity (m/s)
x	Axial position
β	Asperity radius (m)
ε	Eccentricity (mm)
μ	Dynamic Viscosity (Pa-s)
ω	Angular Velocity (rad/s)
Φ_p	Patir and Cheng pressure factor
Φ_s	Patir and Cheng flow factor
σ	Surface Roughness (m)

REFERENCES

[1] EC, 2009. Regulation no 443/2009, setting emission performance standards for new passenger cars as part of the community's integrated approach to reduce co2 emissions from light-duty vehicles. Tech. rep.

[2] Tormos, B., Ramírez, L., Johansson, J., Björling, M., and Larsson, R., 2017. "Fuel consumption and friction benefits of low viscosity engine oils for heavy duty applications". Tribology International, 110, pp. 23–34.

[3] Tomanik, E., 2008. "Friction and wear bench tests of different engine liner surface finishes". Tribology International, 41, pp. 1032–1038.

[4] Will, F., and Boretti, A., 2011. "A new method to warm up lubricating oil to improve the fuel efficiency during cold start". SAE International, 4(2011-01-0318), pp. 175–187.

[5] Dowson, D., Taylor, C. M., and Yang, L., 1996. "Friction modelling for internal combustion engines". Tribology Series, 31, pp. 301–318.

[6] Dubois, G., and Ocvirk, F., 1953. "Analytical derivation and experimental evaluation of short bearing approximation for full journal bearings"'. NACA Techn. Note, 1157.

[7] Taraza, D., and Henein, N., 2000. "Friction losses in multi-cylinder diesel engines". SAE Tecnical Paper (2000-01- 0921).

[8] Liu1, C., Lu1, Y.-J., Zhang, Y.-F., Li1, S., and Müller, N., 2017. "Numerical study on the lubrication performance of compression ring-cylinder liner system with spherical dimples". Plos One, 12.

[9] Avan, E., Spencer, A., Dwyer-Joyce, R., Almqvist, A., and Larsson, R., 2013. "Experimental and numerical investigations of oil film formation and friction in a piston ring-liner contact". Proceedings of the Institution of Mechanical Engineers, Part J: Journal of Engineering Tribology, 227, pp. 126–140.

[10] Tomanik, E., 1996. "Piston ring conformability in a distorted bore". SAE Technical Paper Series (960356).

[11] Bhatt, D., Bulsara, M., and Mistry, K., 2009. "Prediction of oil film thickness in piston ring - cylinder assembly in an IC engine: a review". World Congress on Engineering, II, pp. 3–6.

[12] Jocsak, J., Wong, V., and Tian, T., 2008. "The Effects of Cylinder Liner Finish on Piston Ring-Pack Friction". ASME 2004 Internal Combustion Engine Division Fall Technical Conference, pp. 841–849.

[13] Allmaier, H., Sander, D. E., and Reich, F. M., 2013. "Simulating friction power losses in automotive journal bearings". Procedia Engineering, 68, pp. 49–55.

[14] Sandera, D. E., Allmaier, H., Priebscha, H. H., Reicha, F. M., Wittb, M., Füllenbachb, T., Skiadasb, A., Brouwerc, L., and Schwarzec, H., 2015. “Impact of high pressure and shear thinning on journal bearing friction”. Tribology International, 81, pp. 29–37.

[15] Calabretta, M., Cacciatore, D., and Carden, P., 2010. “Valvetrain friction modeling, analysis and measurement of an high performance engine valvetrain system”. SAE International Paper(2010-01-1492).

[16] Rahnejat, H., Delprete, C., and Magro, L., 2012. “Assessment of friction for cam-roller follower valve train system subjected to mixed non-Newtonian regime of lubrication”. Proceedings of the Spring Technical Conference of the Internal Combustion Division.

[17] Downson, D., and Higginson, G. R., 1966. “Elastohydrodinamic lubrication, the fundamentals of roller and gear lubrication”. Pergamon Press.

[18] Moes, H., 1992. “Optimum similarity analysis with applications to elastohydrodinamic lubrication”. Wear, 159, pp. 57– 66.

[19] Masjedi, M., and Khonsari, M. M., 2012. “Film thickness and asperity load formulas for line-contact elastohydrodinamic lubrication with provision for surface roughness”. J Tribology-T Asme, 134.

[20] Krishnan, A., 2014. “Simulation of an engine friction strip test”. Master’s thesis, Chalmers University of Tecnhology. [21] Emrich, M., and Takats, M., 2016. “Detail engine friction estimation using experimentally-simulation approach”.
International Scientific Conference of The Czech and Slovak Universities and Institutions Dealing with Research of Internal Combustion Engines.

[22] Payri, F., Lujan, J. M., Martin, J., and Abbad, A., 2010. “Digital signal processing of in-cylinder pressure for combustion diagnosis of internal combustion engines”. Mech Syst Signal Process, 6, pp. 1767–1784.

[23] GT-Suite, 2018. Mechanics Theory Manual.

[24] Gohar, R., and Rahnejat, H., eds., 2008. Fundamentals of Tribology. Imperial College Press.
[25] Pulkrabek, W. W., 2004. Engineering fundamentals of the internal combustion engine. Prentice Hall.

[26] Keribar, R., Dursunkaya, Z., and Flemming, M. F., 1991. “An integrated model of ring pack performance”. Transactions of the ASME, 113, pp. 382–389.

[27] Mufti, R. A., and Priest, M., 2009. “Effect of engine operating conditions and lubricant rheology on the distribution of losses in an internal combustion engine”. Journal of Tribology, 131, pp. 382–389.

[28] Notay, R., Priest, M., and Fox, M., 2019. “The influence of lubricant degradation on measured piston ring film thickness in a fired gasoline reciprocating engine”. Tribology International, 129, pp. 112–123.

[29] Patir, N., and Cheng, H. S., 1978. “An average flow model for determining effects of three-dimensional roughness on partial hydrodynamic lubrication”. Transactions of the ASME, 100, pp. 12–17.

[30] Patir, N., and Cheng, H. S., 1979. “Application of average flow model to lubrication between rough sliding surfaces”. Transactions of the ASME, 101, pp. 220–229.

[31] Broatch, A., Olmeda, P., García, A., and Salvador-Iborra, J., 2017. “Impact of swirl on in-cylinder heat transfer in a light-duty diesel engine”. Energy, 119, pp. 1010–1023.

[32] Olmeda, P., García, A., Monsalve-Serrano, J., and et a´l, 2018. “Experimental investigation on RCCI heat transfer in a light-duty diesel engine with different fuels: Comparison versus conventional diesel combustion”. Applied Thermal Engineering, 144, pp. 424–436.

[33] Ali, M., Xianjun, H., Turkson, R. F., and Ezzat, M., 2016. “An analytical study of tribological parameters between piston ring and cylinder liner in internal combustion engines”. Proceedings of the Institution of Mechanical Engineers, Part K: Journal of Multi-body Dynamics, 230, pp. 329–349.

[34] Greenwood, J., and Tripp, J., 1970. “The contact of two nominally flat rough surfaces”. Proceedings of the Institution of Mechanical Engineers, 185, pp. 625–633.

[35] Tomanik, E., Chacon, H., and G.Teixeira, 2003. “A simple numerical procedure to calculate the input data of Greenwood-Williamson model of asperity contact for actual engineering surfaces”. Tribological Research and Design for Engineering Systems, pp. 205–215.

[36] HU, Y., Meng, X., and Xie, Y., 2018. “A new efficient flow continuity lubrication model for the piston ring-pack with consideration of oil storage of the cross-hatched texture”. Tribology International, 119, pp. 443–463.

[37] Glidewell, J., and Korcek, S., 1998. “Piston ring / cylinder bore friction under flooded and starved lubrication using fresh and aged engine oils”. SAE International (982659).

[38] Littlefair, B., la Cruz, M. D., Theodossiades, S., Mills, R., Howell-Smith, S., Rahnejat, H., and Dwyer-Joyce, R., 2014. “Transient tribo-dynamics of thermo-elastic compliant high-performance piston skirts”. Tribology Letters, 53, pp. 51–70.

[39] McClure, F., and Tian, T., 2008. “Simplified piston secondary motion model considering the dynamic and static deformation of piston skirt and cylinder bore in internal combustion engines”. SAE Technical Paper (2008-01-1612).

[40] Keribar, R., and Dursunkaya, Z., 1992. “A comprehensive model of piston skirt lubrication”. SAE Technical Paper Series(920483).

[41] Balakrishnan, S., and Rahnejat, H., 2005. “Isothermal transient analysis of piston skirt-to-cylinder wall contacts under combined axial, lateral and tilting motion”. Journal of Physics D: Applied Physics, 38.

[42] Goenka, P. K., 1984. “Analytical curve fits for solution parameters of dynamically loaded journal bearings”. Journal of Tribology, 106, pp. 421–427.

[43] Raimondi, A. A., and Boyd, J., 1958. “A solution for the finite journal bearing and its application to analysis and design: I”. ASLE Transactions, 1, pp. 159–174.

[44] Taylor, C. M., 1993. Engine Tribology. Elsevier.

[45] Hertz, H., 1882. “über die berührung fester elastischer köper (on the contact of elastic solids)”. Journal für die reine und angewandte Mathematik, 92, pp. 156–171.

[46] Teodorescu, M., Taraza, D., Henenin, N. A., and W. Bryzik, 2003. “Simplified elasto-hydrodynamic friction model of the cam-tappet contact”. SAE Technical Paper(2003-01-0985).

[47] Guo, J., Zhang, W., and Zou, D. 2011. “Investigation of dynamic characteristics of a valve train system”. Mechanism and Machine Theory, 46, pp. 1950–1969.

[48] van Leeuwen, H., 2009. “The determination of the pressure-viscosity coefficient of a lubricant through an accurate film thickness formula and accurate film thickness measurements”. Proceedings of the Institution of Mechanical Engineers Part J Journal of Engineering Tribology 1994-1996, 8, pp. 208–210.

[49] Moes, H., 1992. “Optimum similarity analysis with applications to elastohydrodinamic lubrication”. Wear, 159, pp. 57– 66.

[50] Tormos, B., Martín, J., Carreño, R., and Ramírez, L., 2018. “A general model to evaluate mechanical losses and auxiliary energy consumption in reciprocating internal combustion engines”. Tribology International, 123, pp. 161– 179.

[51] Irimescu, A., Iorio, S. D., Merola, S. S., Bianca, P. S., and Vaglieco, M., 2018. “Evaluation of compression ratio and blow-by rates for spark ignition engines based on in-cylinder pressure trace analysis”. Energy Conversion and Management, 162, pp. 98–108.

[52] Söderfjäll, M., Almqvist, A., and Larsson, R., 2016. “A model for twin land oil control rings”. Tribology International,95, pp. 475–482.

[53] Gebretsadik, D., Hardell, J., and Prakash, B., 2015. “Friction and wear characteristics of different pb-free bearing materials in mixed and boundary lubrication regimes”. Wear, 340-341, pp. 63–72.

Figure Captions List

Table Caption List

Table 1. 4 strokes DI-Diesel engine characteristics

Feature Description	Description
Cylinders	4 in-line
Bore (mm)	80.02
Stroke (mm)	79.5
Total displacement (cm^3)	1598
Air management	Turbocharged
Maximum Power (kW)	96 @ 3500 rpm
Maximum Torque (N-m)	320 @ 1750 rpm
Injection	Common rail
Valvetrain	Cam-follower

Table 2. Lubricant properties

Oil properties (5W30)	**Value**
Kinematic Viscosity @40ºC (cSt)	62
Kinematic Viscosity @100ºC (cSt)	10.4
Density @15ºC (g/ml)	0.861

Table 3. Parameters used in Greenwood-Tripp model

	σβη	**σ/β**	**η(1/m^2)**	**E(GPa)**	**υ**
Fire Ring	0.059	0.0028	$1.02 \cdot 10^9$	200	0.285
Compression Ring	0.044	0.0021	$1.02 \cdot 10^9$	200	0.285
Oil ring	0.044	0.0021	$1.02 \cdot 10^9$	200	0.285
Piston Skirt	0.059	0.0028	$1.04 \cdot 10^9$	200	0.285
Cylinder	0.093	0.0069	$1.02 \cdot 10^9$	126.5	0.25
Bearings	0.061	0.0012	$4 \cdot 10^9$	71	0.33
Camshaft	0.025	0.0009	$1.04 \cdot 10^9$	200	0.285

Table 4. Bearings geometry

	Main Bearings	**Con-rod Bearings**
Diameter (mm)	51.48	51.58
Width (mm)	17.8	21.1
Clearance (mm)	0.025	0.025
Material	Al-Sn-Cu-Ni	Al-Sn-Cu-Ni

Table 5. Auxiliaries coefficients

	Oil	**Cool**	**Fuel**
k_1	1.700583	$3.97 \cdot 10^{-5}$	$1.41 \cdot 10^{-3}$
k_2	$8.07 \cdot 10^{-3}$	0.05657	-
k_3	0.64	-	-

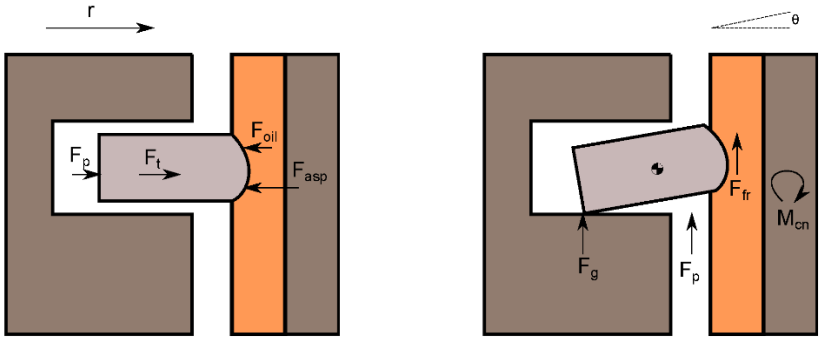

Figure 1. Forces balance in piston-ring assembly.

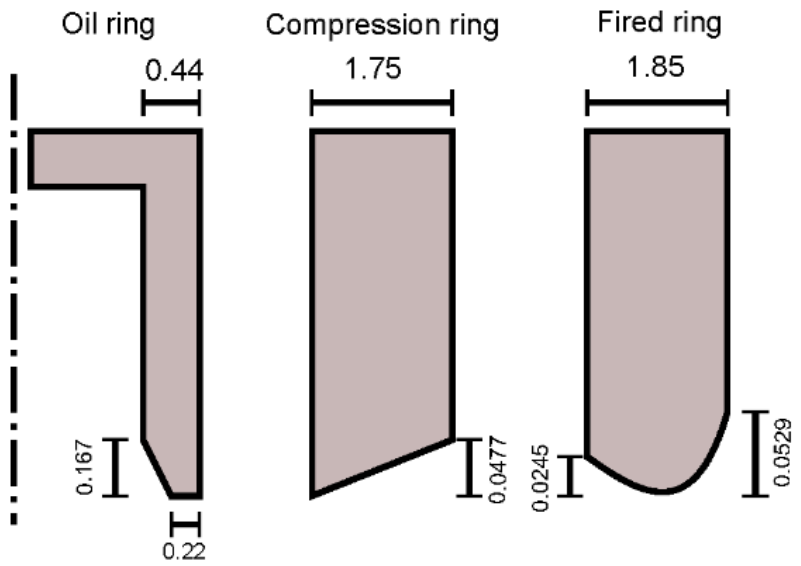

Figure 2. Ring profiles used in the engine.

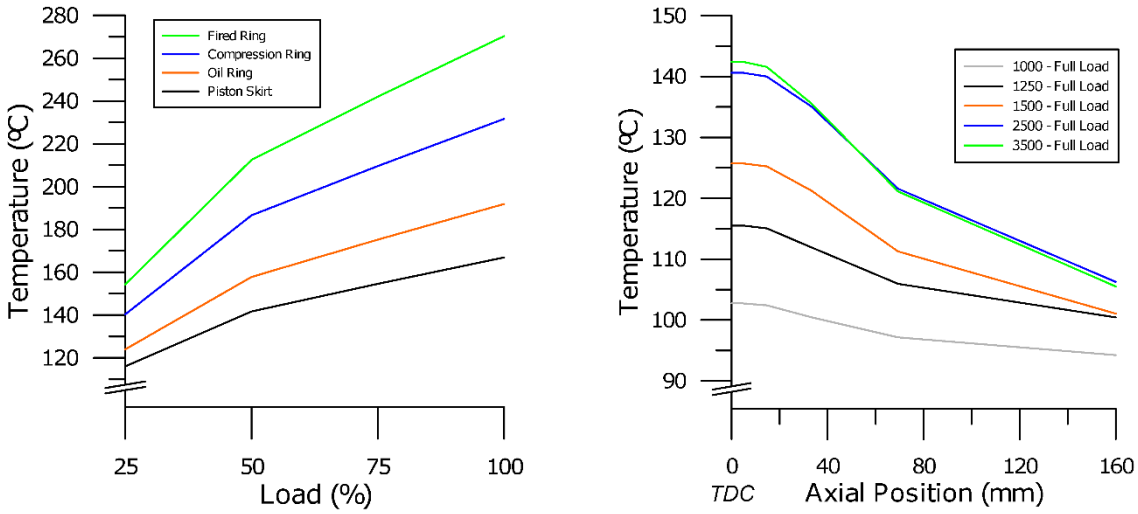

Figure 3. Left: Temperature on rings. Right: Variation of temperature on cylinder.

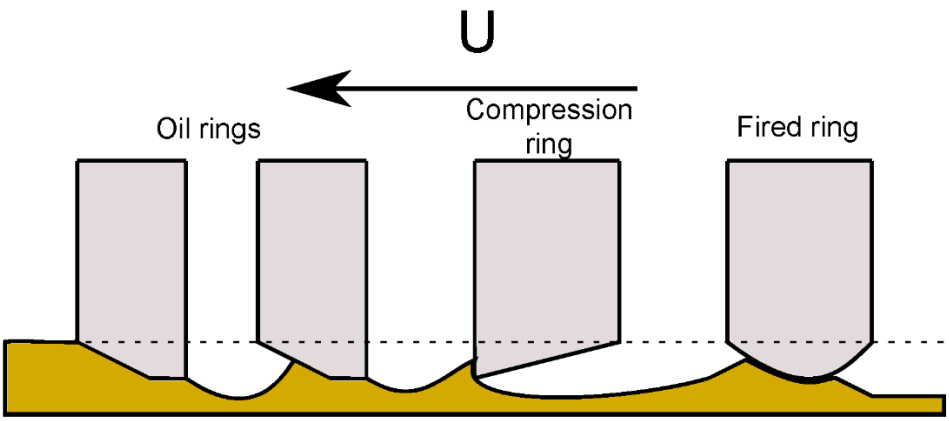

Figure 4. Partially-flooded condition.

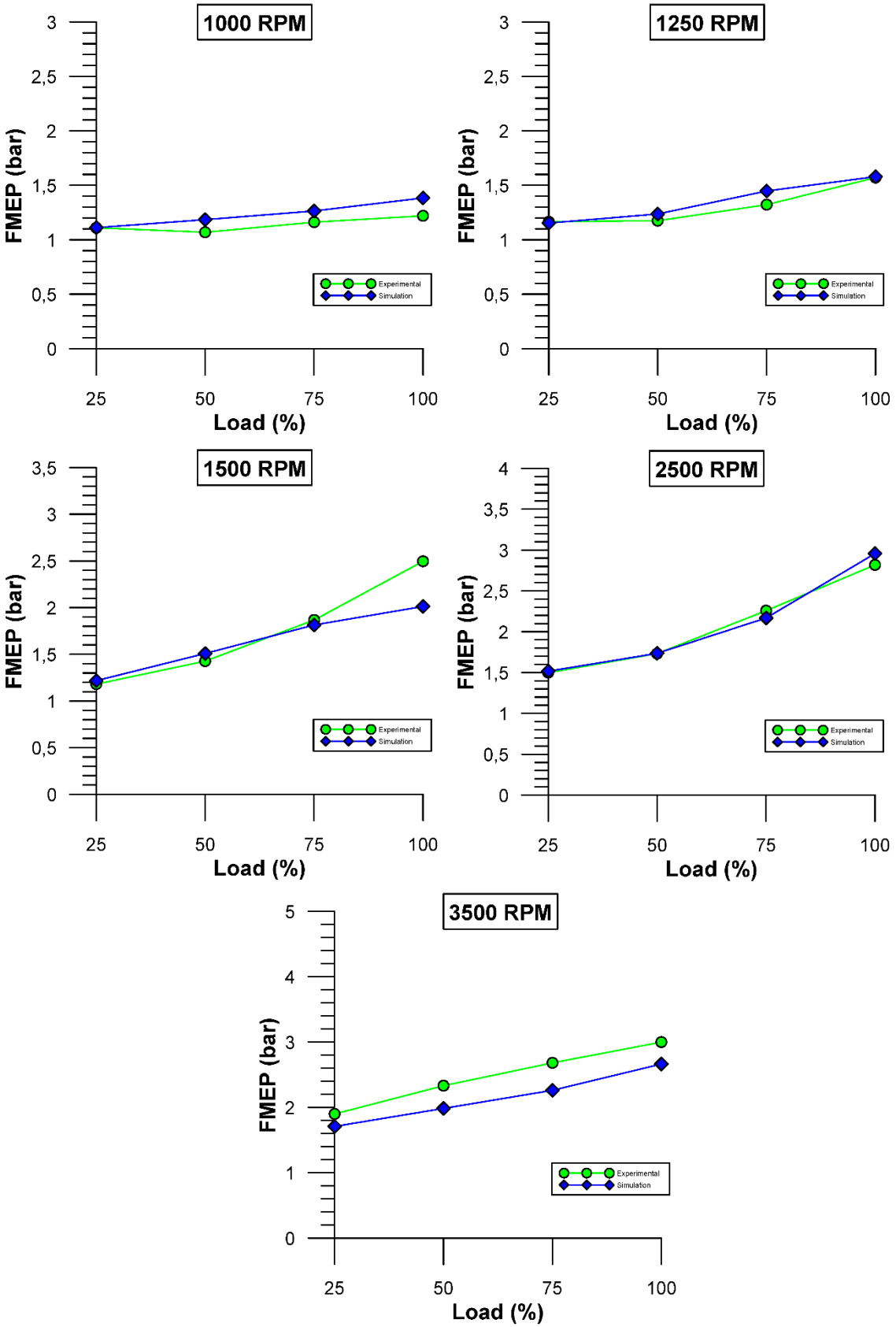

Figure 5. Experimental versus modeled results.

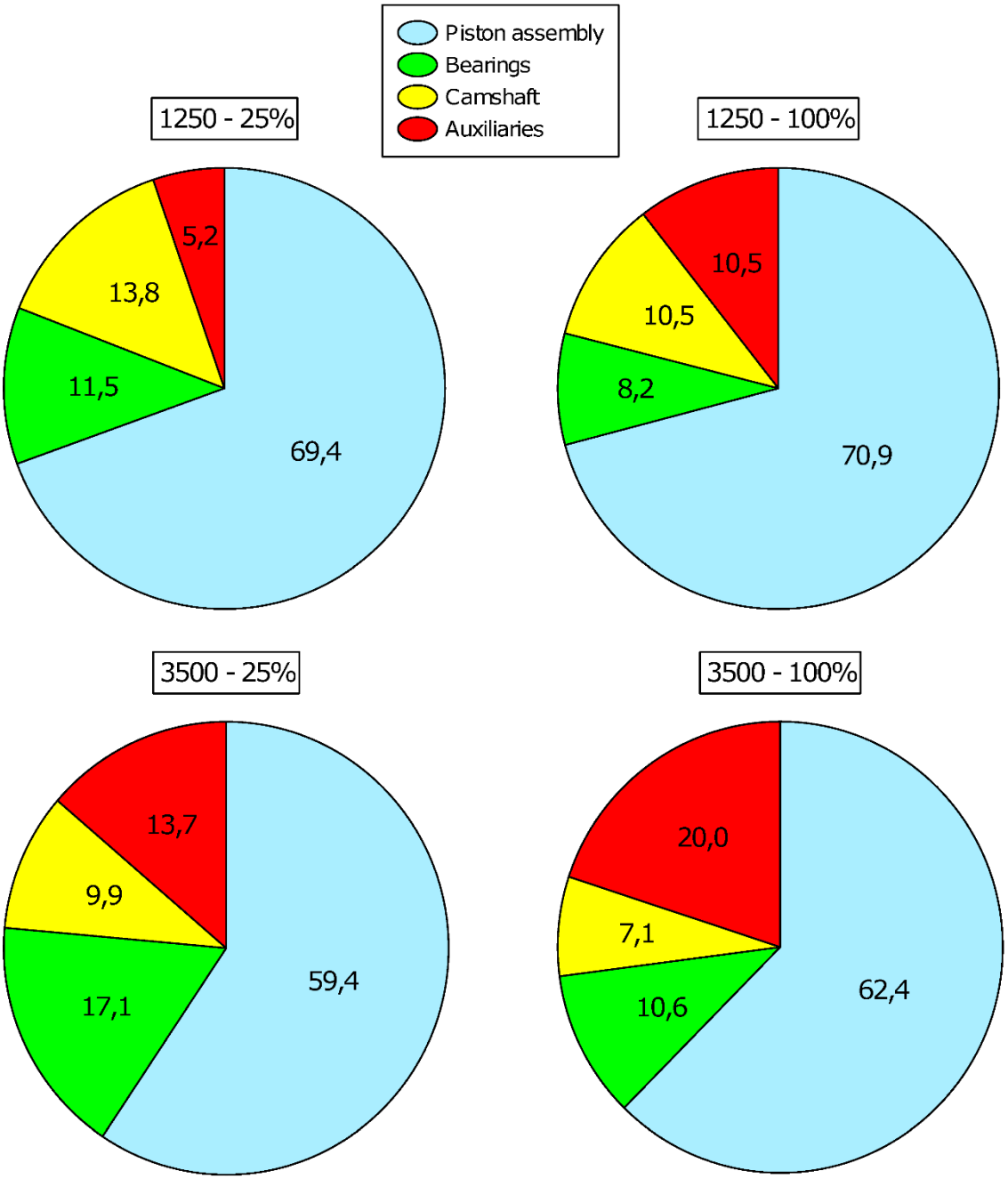

Figure 6. Mechanical losses distribution.

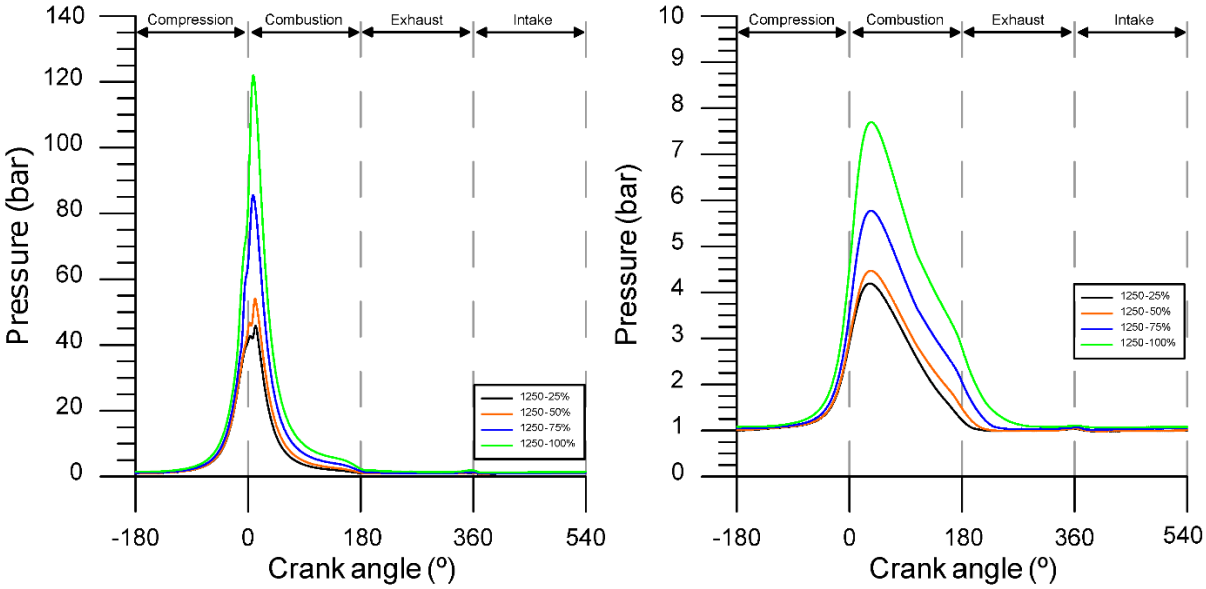

Figure 7. Left: Pressure in upper land ring and groove land ring. Right: Pressure in bottom land ring. For fired ring.

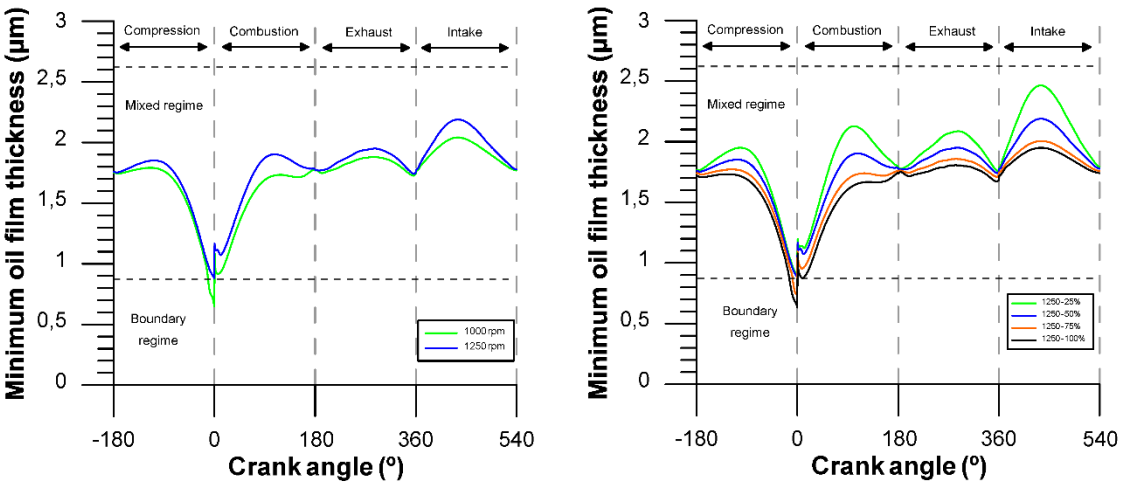

Figure 8. Left: MOFT at same engine load. Right: MOFT at same engine speed.

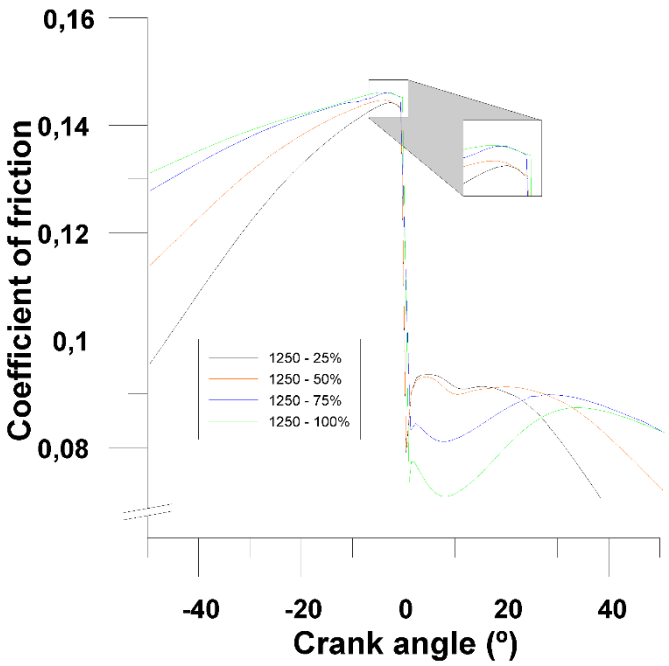

Figure 9. Coefficient of friction.

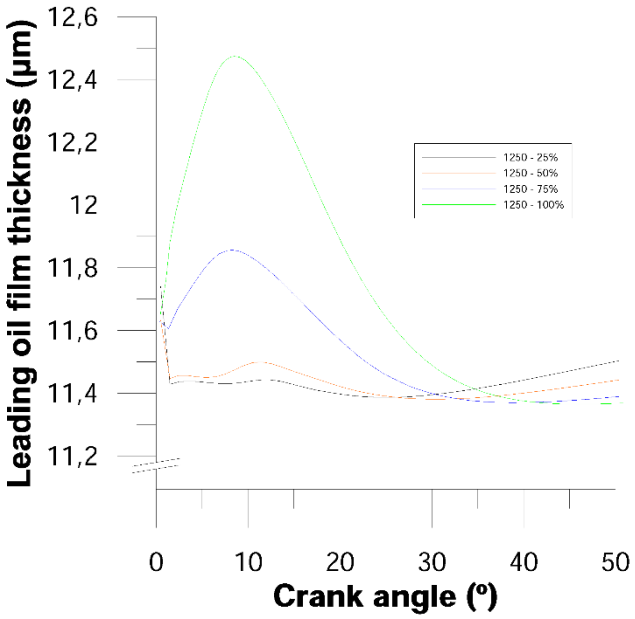

Figure 10. Oil film thickness available at leading point of the ring.

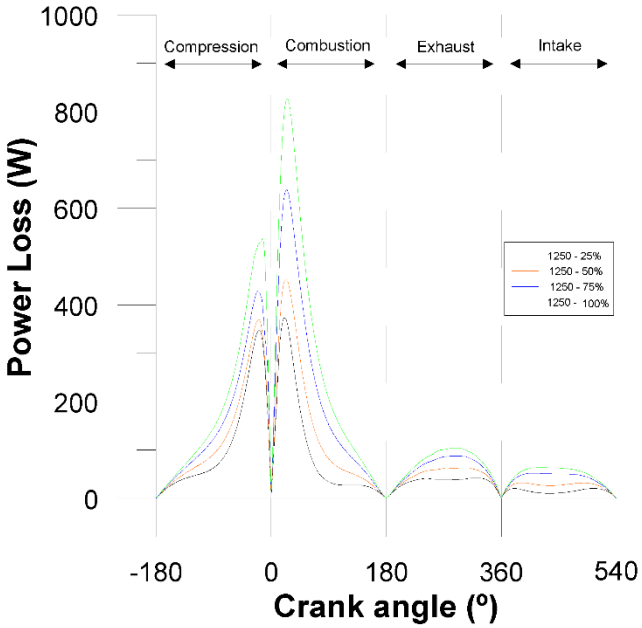

Figure 11. Power losses in fire ring @1250 rpm.

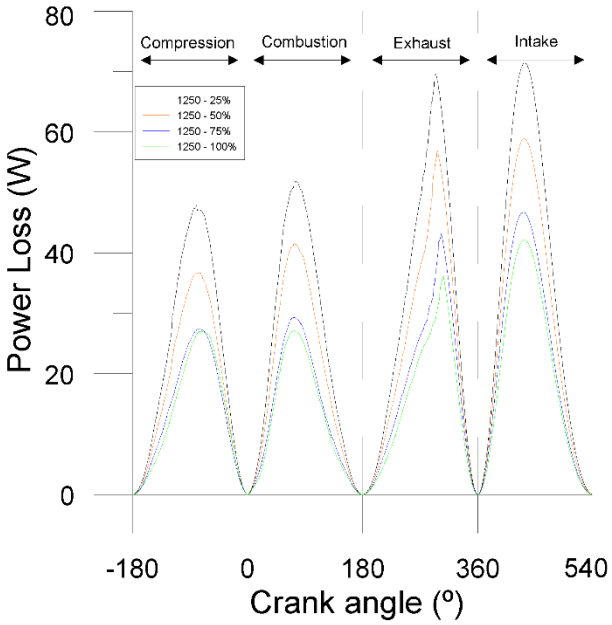

Figure 12. Power losses in piston skirt@1250 rpm.

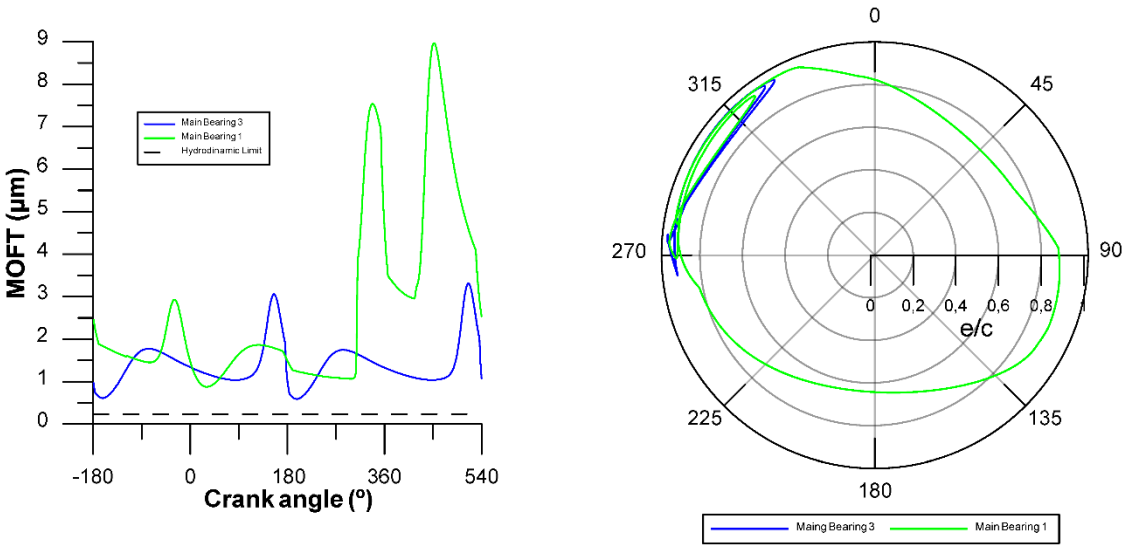

Figure 13. Left: MOFT. Right: Journal orbit for main bearings 1 and 3.

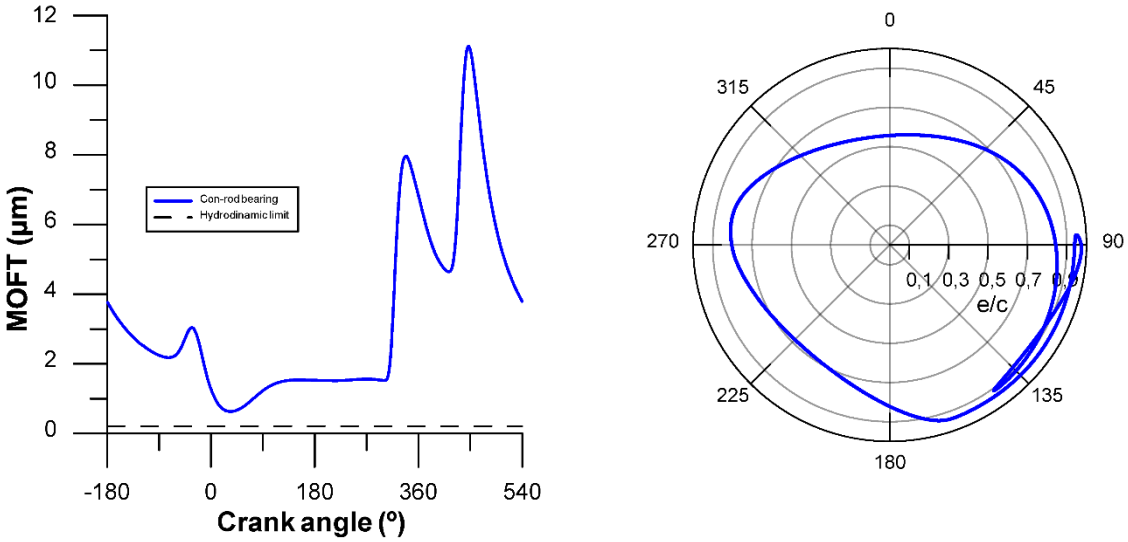

Figure 14. Left: MOFT. Right: Journal orbit for con-rod bearings.

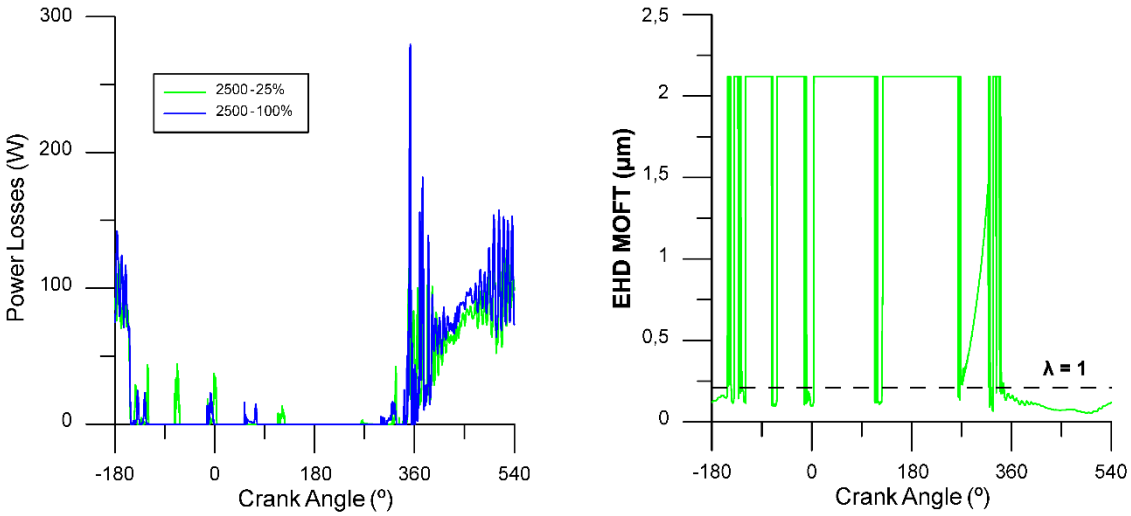

Figure 15. Left: Power losses in cam-follower. Right: MOFT.

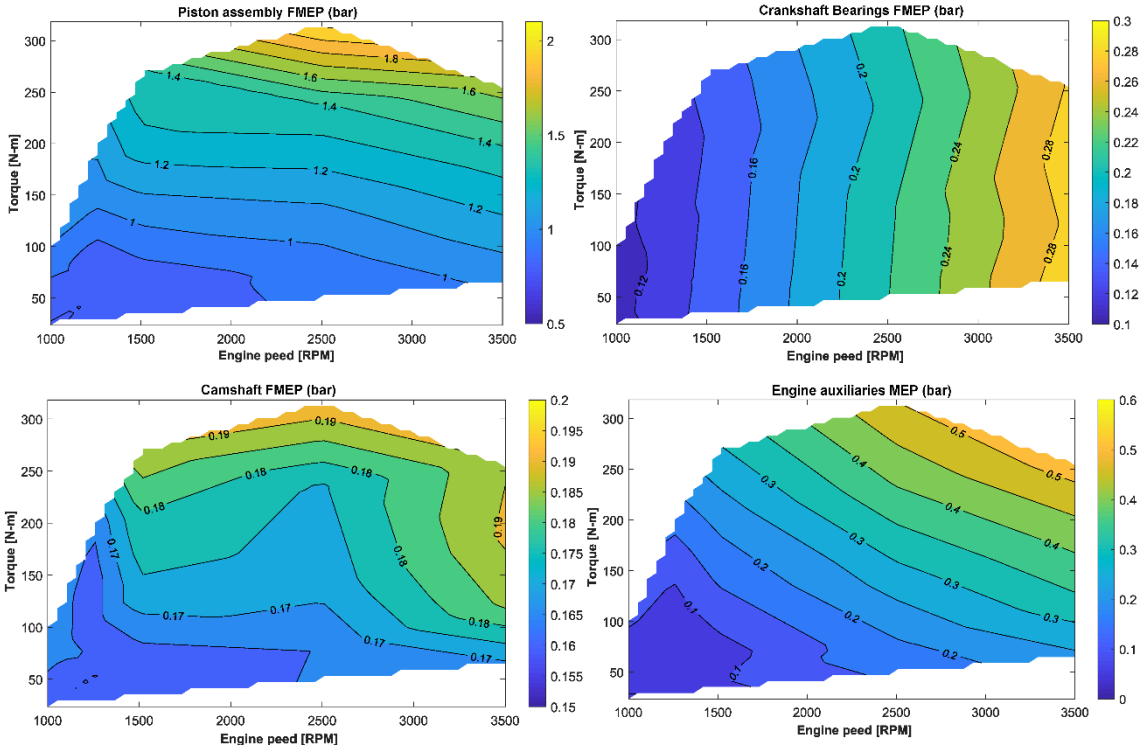

Figure 16. Engine friction maps.